Supporting Information

Surface-defect engineering of nickel hexacyanoferrate material for high-performance printed flexible supercapacitor

Jing Liang[a], Bin Tian[a], Xinyu Zhang[a], Changzhong Jiang[b], Dong He[c*] and Wei Wu[a*]

[a] Laboratory of Printable Functional Materials and Printed Electronics, School of Printing and Packaging, Wuhan University, Wuhan 430072, P. R. China

[b] College of Materials Science and Engineering, Hunan University, Changsha 410000, P. R. China

[c] Department of Physics, Key Laboratory of Artificial Micro- and Nano-structures of Ministry of Education, Hubei Nuclear Solid Physics Key Laboratory, Wuhan University, Wuhan, 430072 P. R. China

[*] Corresponding author：weiwu@whu.edu.cn (W. Wu)

Materials characterization

Scanning electron microscopy (SEM) and energy dispersive X-ray (EDX) spectrometry mapping images were performed by using a Hitachi S-4800 scanning electron microscopy. The morphological analysis of the synthesized samples was studied by high resolution transmission electron microscopy (HRTEM) (FEI Tecnai F20 200 kV) imaging. The electrodes were quantified using inductively coupled plasma mass spectrometry (ICP-MS) (Agilent 7900, Agilent Technology, Santa Monica, CA, USA). X-ray diffraction (XRD) data was obtained in the range from 2° to 140° in 24 h using a D8 Advance X-ray diffractometer with Cu Kα X-ray source. X-ray photoelectron spectroscopy (XPS) information was collected by X-ray photoelectron spectroscopy (ESCALAB250Xi, Thermo Fisher Scientific). Fourier transform infrared (FTIR) spectra were obtained using a NICOLET 5700 spectroscopy system. The specific surface area was determined by the Brunauer-Emmett-Teller (BET) analysis from the N_2 adsorption/desorption isotherms (Micromeritics, ASAP 2460). The pore size distributions were analyzed using the Barrett-Joyner-Halenda (BJH) method. The rheological properties of formulated ink were performed by using the Rheometer (AR2000ex rotary rheometer, TA).

Electrochemical measurement

All electrochemical tests (cyclic voltammetry (CV), galvanostatic charge-discharge (GCD), and electrochemical impedance spectroscopy (EIS)) were performed on a CHI 760E electrochemical workstation (CH Instruments Inc. Shanghai, China) at room temperature. For the three-electrode test, the work electrodes were prepared with 75 wt% active electrode materials, 10 wt% acetylene black and 15 wt% PVDF. Then, the obtained slurry evenly coated on the surface of clean nickel foam for 1×1 cm^2. After drying in a 100 ℃ for 4 hours and pressing at 8 MPa pressure for about 10 seconds, the working electrode is successfully prepared. The mass loading of all the cathode electrodes was controlled as 1 mg cm^{-2}. The Ag/AgCl and carbon electrode were used as the reference electrode and counter electrode, respectively. And 0.5 M solution of Na_2SO_4 was used as the electrolyte. The measurement of NiHCF-etching-based printed flexible supercapacitor with symmetric electrodes are tested by a two-electrode method.

The cycle stability was performed by using a multichannel battery testing system (LAND CT2001A).

Theoretical calculations

Density functional theory (DFT) calculations were carried out using CASTEP code in materials studio. We choose the Perdew-Burke-Ernzerhof (PBE) functional of generalized gradient approximation (GGA) as the electronic exchange-correlation potential. Furthermore, the ultrasoft pseudopotentials were used and the kinetic energy cutoff of the plane-wave basis set was set to 450 eV. Brillouin zone integration was sampled with the 1×1×1 MonkhorstPack mesh K-point for calculations, respectively. During the calculation, the $Ni_4Fe_4C_{24}N_{24}$ supercell was constructed for the sample of NiHCF and $Ni_4Fe_3C_{18}N_{18}$ for NiHCF-etching materials. The convergence tolerances for energy, maximum displacement and maximum force were set to 2×10^{-5} eV/atom, 2×10^{-3} Å and 0.05 eV $Å^{-1}$ during geometry optimization, respectively. The transition state searching was performed by a complete linear synchronous transition (LST) and quadratic synchronous transitions (QST) approach.

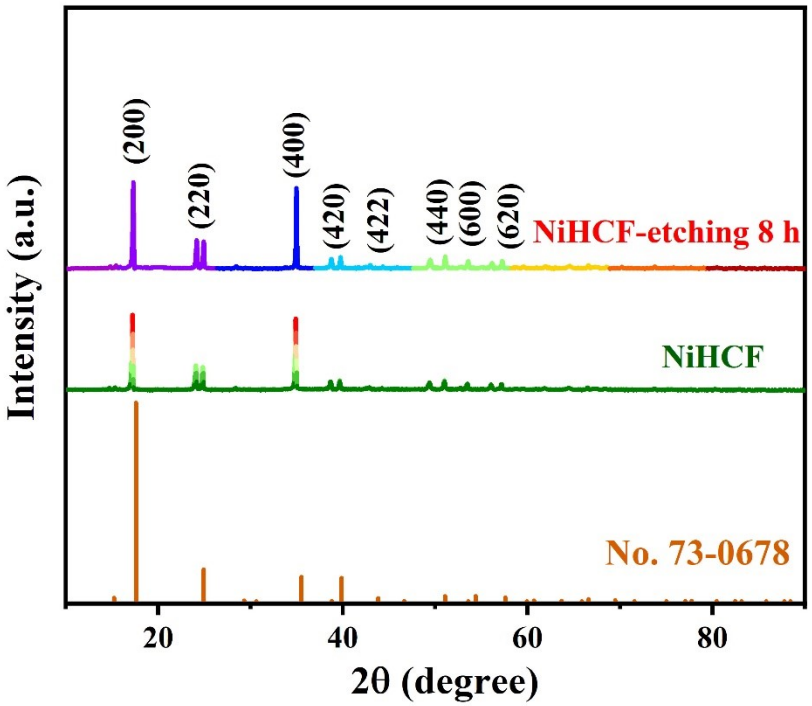

Fig. S1 XRD patterns of NiHCF and NiHCF-etching 8 h electrode materials.

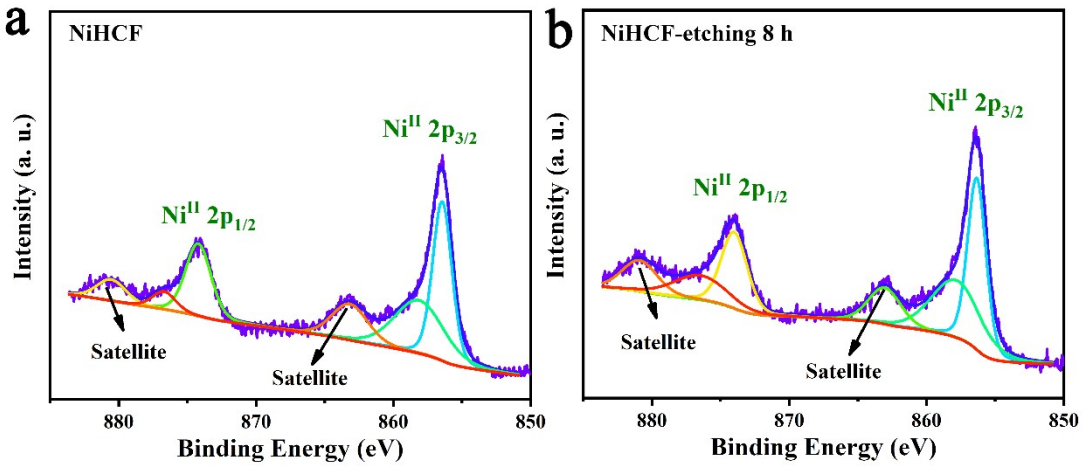

Fig. S2 The Ni 2p XPS spectrum of (a) NiHCF and (b) NiHCF-etching 8 h electrode materials.

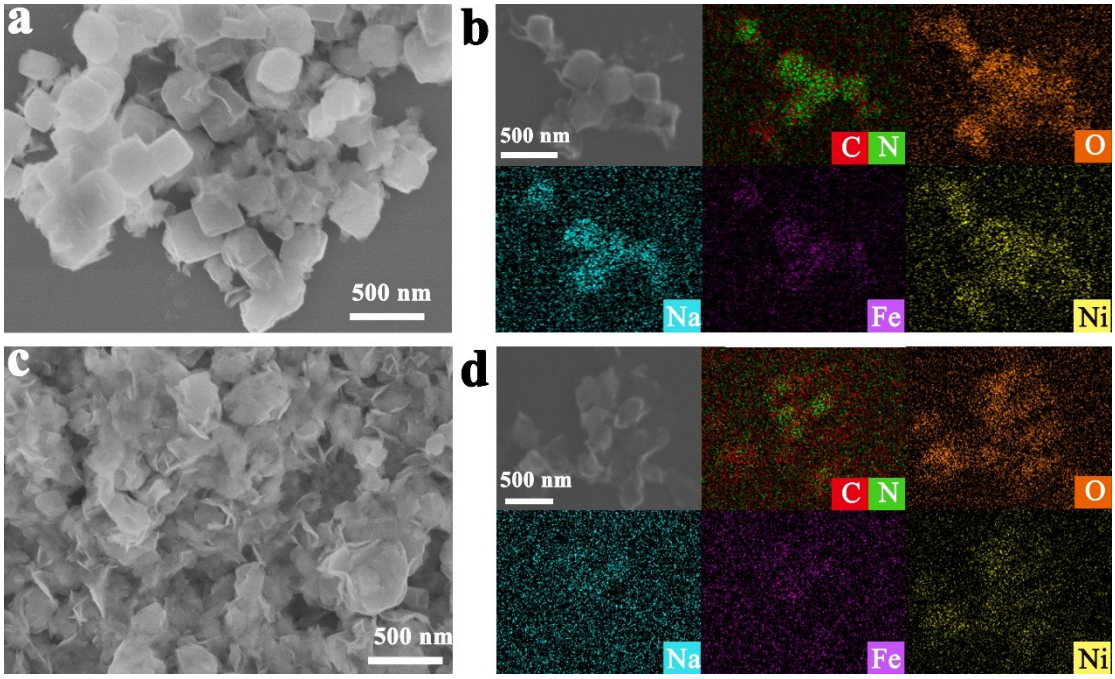

Fig. S3 (a, c) SEM images and (b, d) EDX element mapping of NiHCF electrode at etching time of 4 h and 12 h.

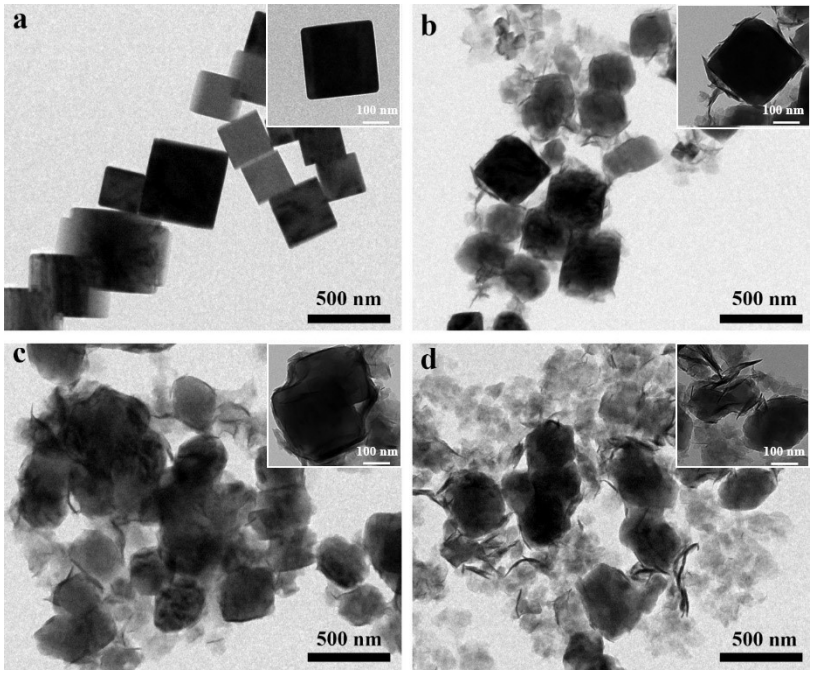

Fig. S4 TEM images of (a) NiHCF, (b) NiHCF-etching 4 h, (c) NiHCF-etching 8 h and (d) NiHCF-etching 12 h, respectively.

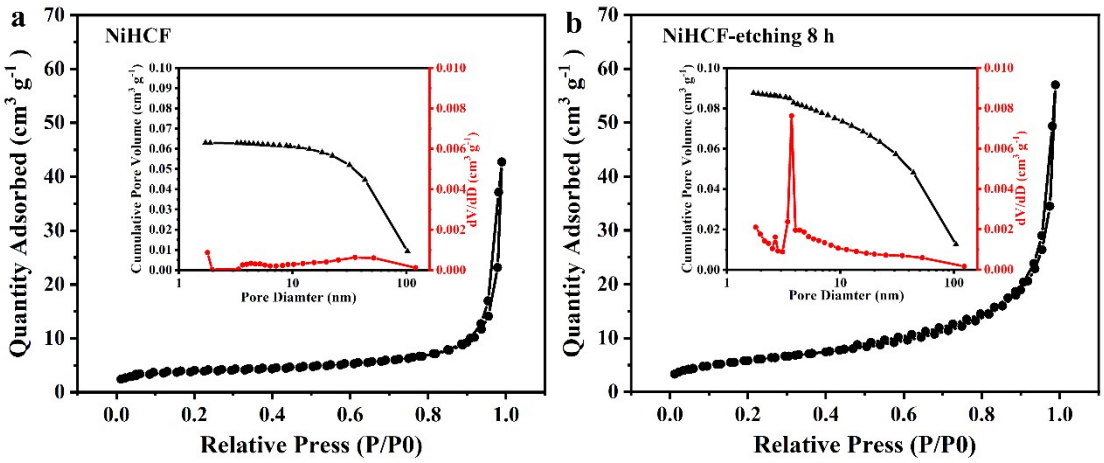

Fig. S5 Brunauer-Emmett-Teller (BET) surface area plots with an inset of the cumulative specific volume and pore size distribution of (a) NiHCF and (b) NiHCF-etching 8 h electrode materials.

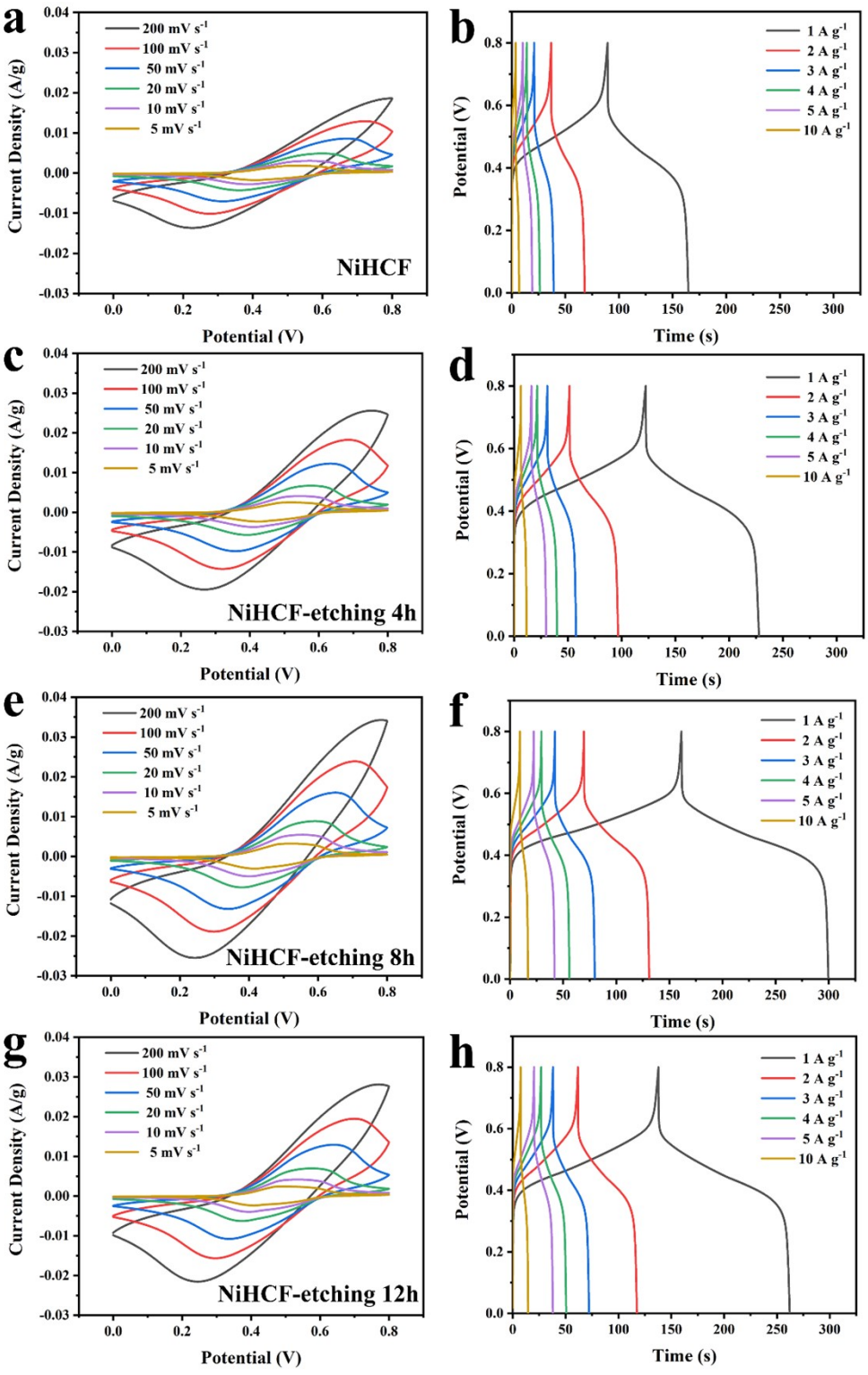

Fig. S6 The CV (scan rate of 5 mV s^{-1}-200 mV s^{-1}) and GCD (current density of 1 A g^{-1}-10 A g^{-1}) curves of NiHCF electrode materials at different etching time (a, b 0 h; c, d 4 h; e, f 8 h; g, h 12 h).

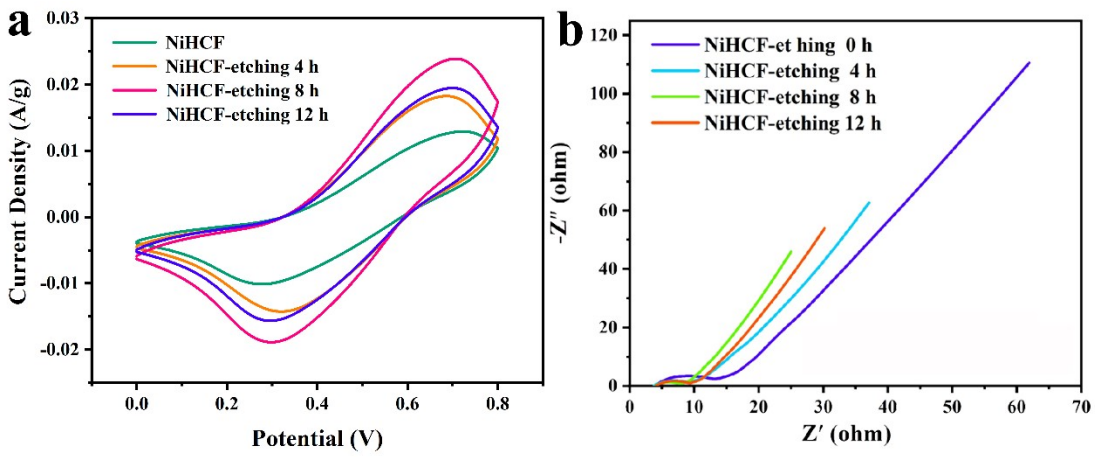

Fig. S7 (a) The CV (scan rate of 100 mV s^{-1}) and (b) EIS (frequency at 10^{-2}-10^{6} Hz) figures of the NiHCF electrode materials.

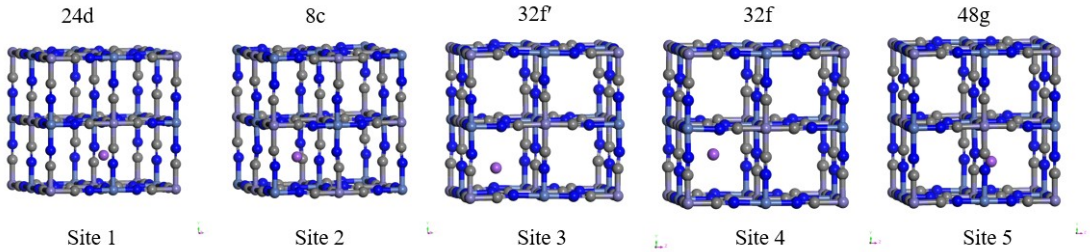

Fig. S8 Potential Na ions adsorption sites and adsorption structure of NiHCF.

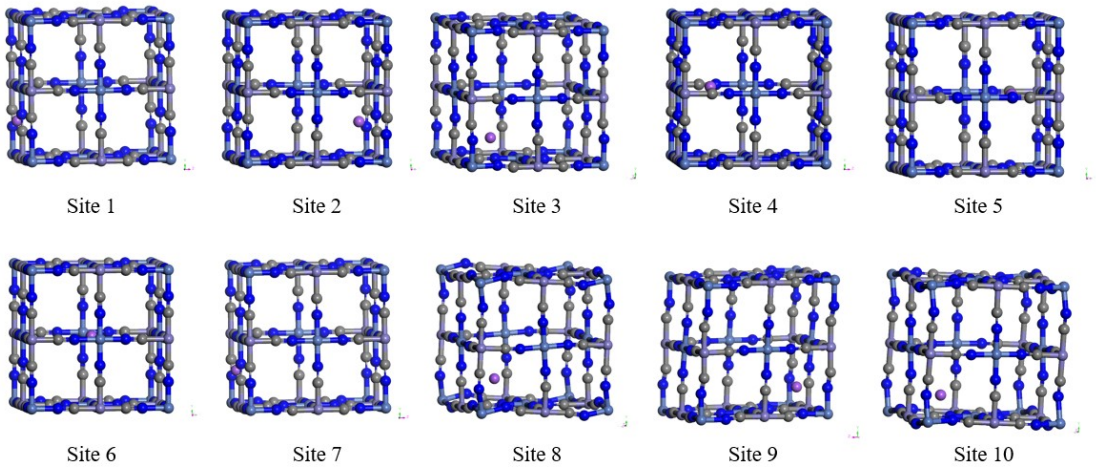

Fig. S9 Potential Na ions adsorption sites and adsorption structure of NiHCF-etching.

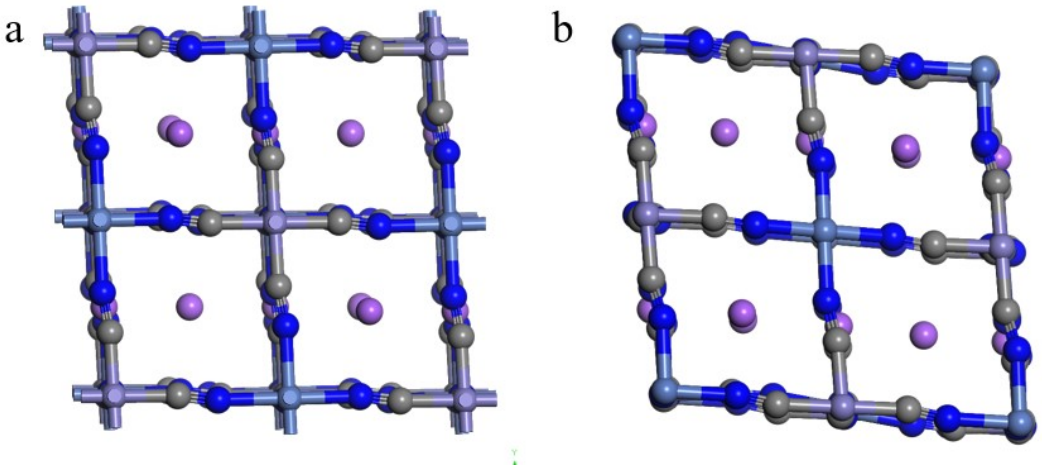

Fig. S10 Structure of Na ions fully embedded in the lattice of (a) NiHCF and (b) NiHCF-etching.

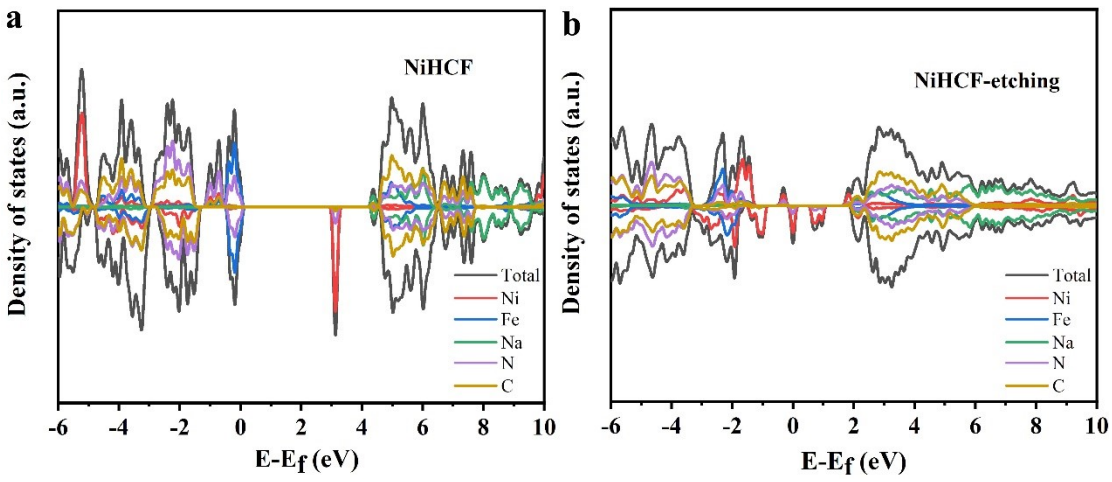

Fig. S11 The calculated partial density of sates (PDOS) patterns of (a) NiHCF and (b) NiHCF-etching.

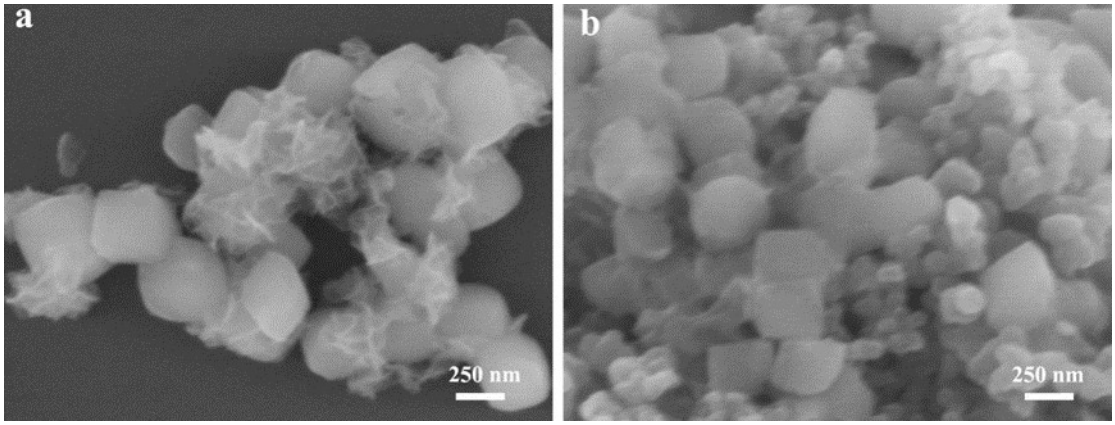

Fig. S12 The SEM images of NiHCF-etching based printed flexible supercapacitor (a) before and (b) after cycling.

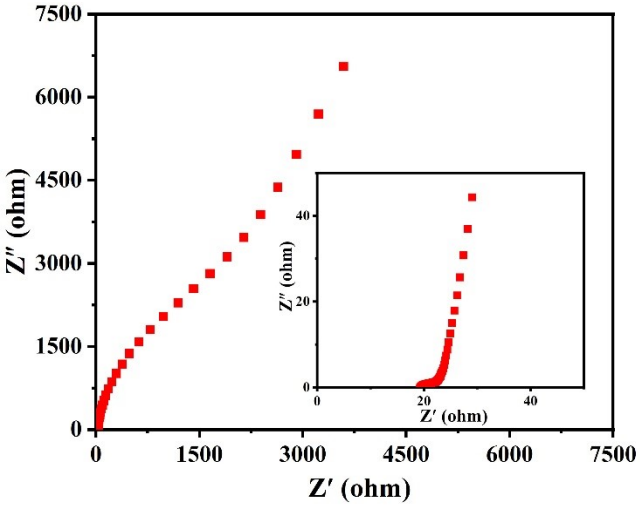

Fig. S13 The EIS plots of NiHCF-etching-8 h based FSCs in PVA/LiCl electrolyte.

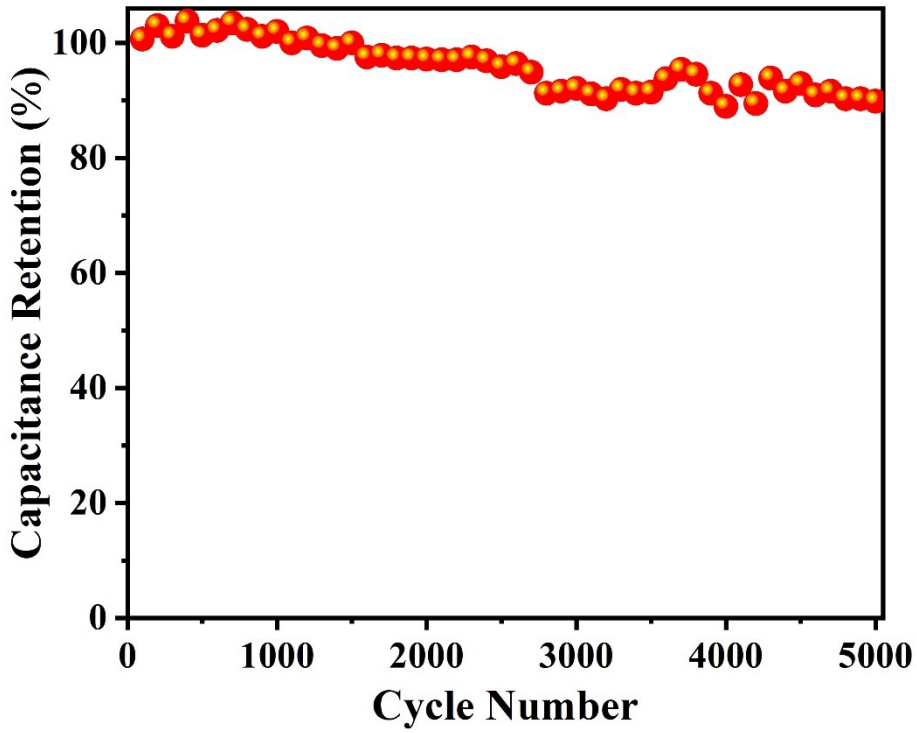

Fig. S14 The cycle performance of NiHCF-based FSCs in PVA/LiCl electrolyte

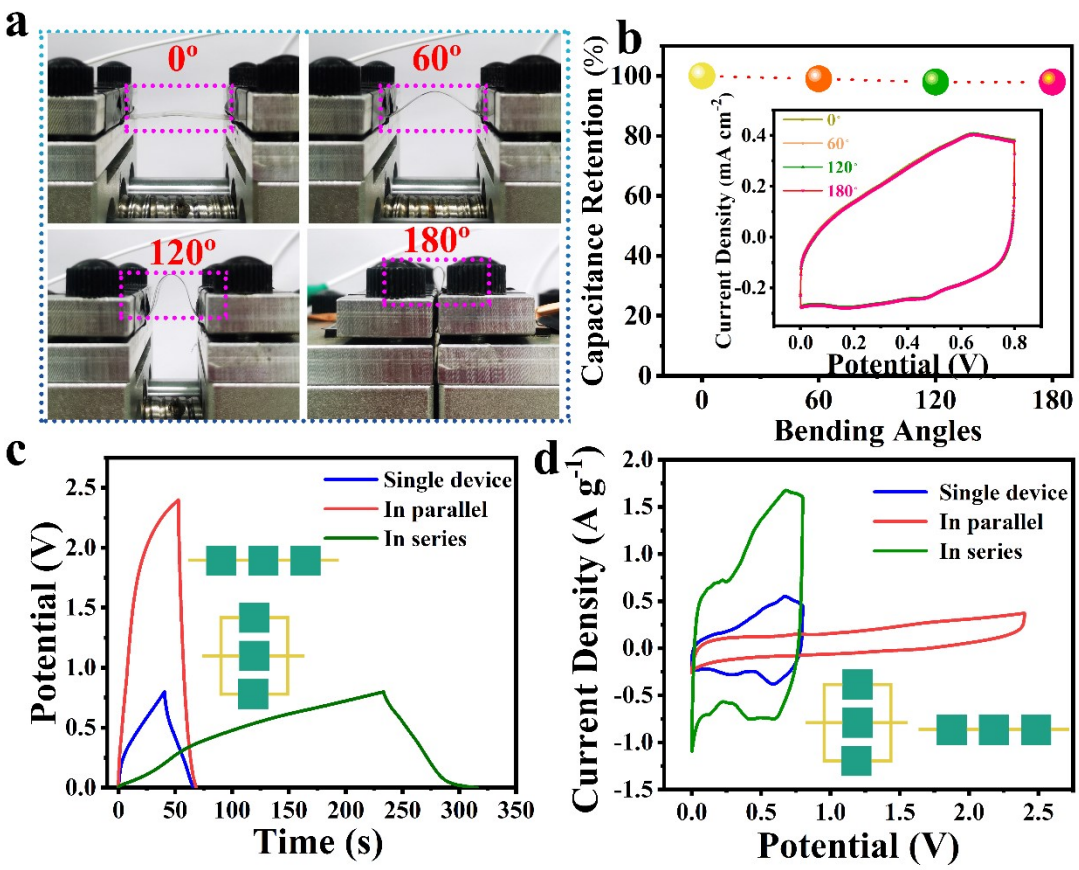

Fig. S15 Integration and application of printed device in PVA/LiCl electrolyte. The (a) optical image and (b) capacitance retention as functional of bending angle (insert is the corresponding CV curves and the supercapacitor at bending state can power an LED) of the flexibility demonstration of printed flexible device at different bending state (0º, 60º, 120º and 180º). (c) GCD (0.1 mA cm^{-2}) and (d) CV curves (100 mV s^{-1}) of the three printed flexible supercapacitors connected in parallel and in series, respectively (Inset is the schematic diagram of parallel and series connections).

Table S1 Structural parameters of the NiHCFs-etching sample obtained from Rietveld analysis.

Atom	*x*	*y*	*z*	Wyckoff	Uiso	Occupancy
Fe	0	0.5	0.5	2d	0.2	0.937
Ni	0	0	0	2a	0.2	1
C1	-0.00399	0.29401	0.31401	4e	0.5	1
C2	0.17401	0.50801	0.51401	4e	0.5	1
C3	-0.00559	0.67481	0.28991	4e	0.5	1
N1	0.00487	0.19847	0.19707	4e	0.5	1
N2	0.30227	0.50407	0.50227	4e	0.5	1
N3	0.00307	0.80637	0.20907	4e	0.5	1
O1	0.23020	0.26820	0.25020	4e	0.5	1
O2	0.24286	0.19686	0.68086	4e	0.5	1
Na	0.25489	0.45135	0.03743	4e	0.2	0.879
S.G. P21/n a = 10.23919, b = 7.37201, c = 7.15318 Å, α=γ=90 β=92.44132						
Rp= 1.53%, Rwp= 2.17%, Rexp=1.90%						

Table S2 ICP-MS results for the NiHCF cube and NiHCF-etching samples.

Sample	Element	Weight%	Atomic%
NiHCF cube	Na	5.26	0.22
	Ni	7.74	0.13
	Fe	6.85	0.12
NiHCF-etching	Na	7.01	0.31
	Ni	6.83	0.17
	Fe	7.98	0.14

Table S3 The relative energy of NiHCF adsorption Na ions at different sites.

NiHCF	Site 1	Site 2	Site 3	Site 4	Site 5
Relative energy (eV)	0	0.325616	0.82579926	0.869969	0.721732

Table S4 The relative energy of NiHCF-etching adsorption Na ions at different sites.

NiHCF-etching	Site 1	Site 2	Site 3	Site 4	Site 5
Relative energy (eV)	0	-0.05293	0.012658	0.424976	1.747532
	Site 6	**Site 7**	**Site 8**	**Site 9**	**Site 10**
	1.44163	0.393933	0.395476	0.630844	0.423722